Electronic Supplementary Material (ESI) for Nanoscale.

SUPPORTING INFORMATION

Synthesis of compositionally tunable, hollow mixed metal sulphide $Co_xNi_yS_z$ octahedral nanocages and their composition-dependent electrocatalytic activities for oxygen evolution reaction

Jun Kim,[ab] Haneul Jin,[b] Aram Oh,[b] Hionsuck Baik,[c] Sang Hoon Joo[d] and Kwangyeol Lee*[ab]

[a]Center for Molecular spectroscopy and Dynamics, Institute for Basic Science (IBS), Seoul 02841, Republic of Korea

[b]Department of Chemistry, Korea University, Seoul 02841, Republic of Korea

[c]Korea Basic Science Institute (KBSI), Seoul 02841, Republic of Korea

[d]School of Energy and Chemical Engineering, Ulsan National Institute of Science and Technology (UNIST), Ulsan 44919, Republic of Korea

E-mail: kylee1@korea.ac.kr

Supplementary Figures

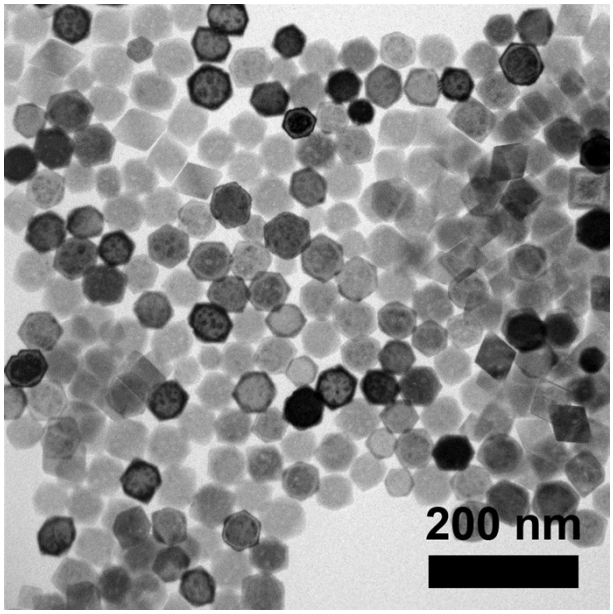

Fig. S1 TEM image of CoO octahedra.

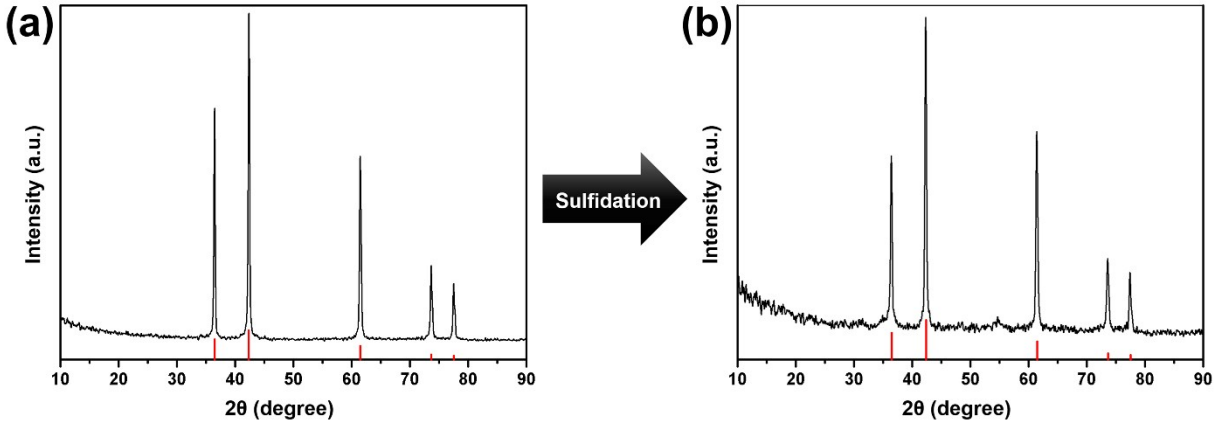

Fig. S2 XRD patterns of (a) CoO octahedral octahedra and (b) CoO@Co_xS_y core-shell octahedra after sulfidation (red vertical lines: CoO reference, JCPDS #01-078-0431).

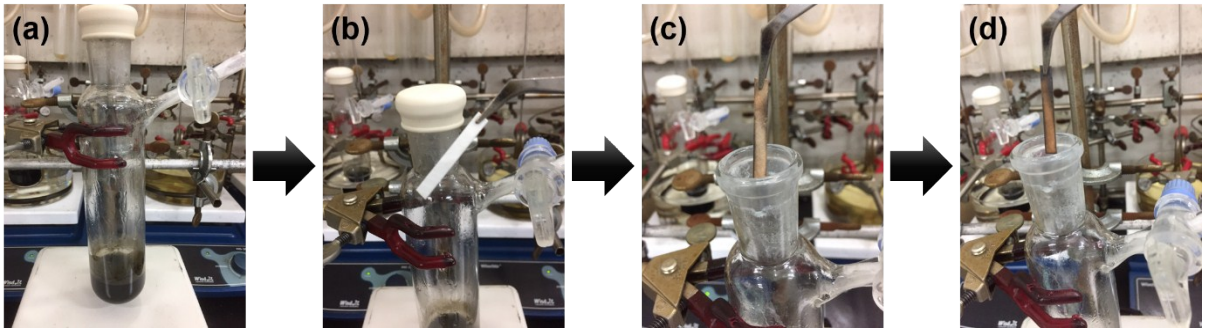

Fig. S3 (a) After the synthesis of $CoO@Co_xS_y$ core-shell octahedra, the tube was cooled to room temperature. (b) A fresh lead acetate strip was prepared and (c) the strip was brought near the mouth of the reaction tube to detect H_2S. (d) The strip instantly turned black indicating the presence of H_2S.

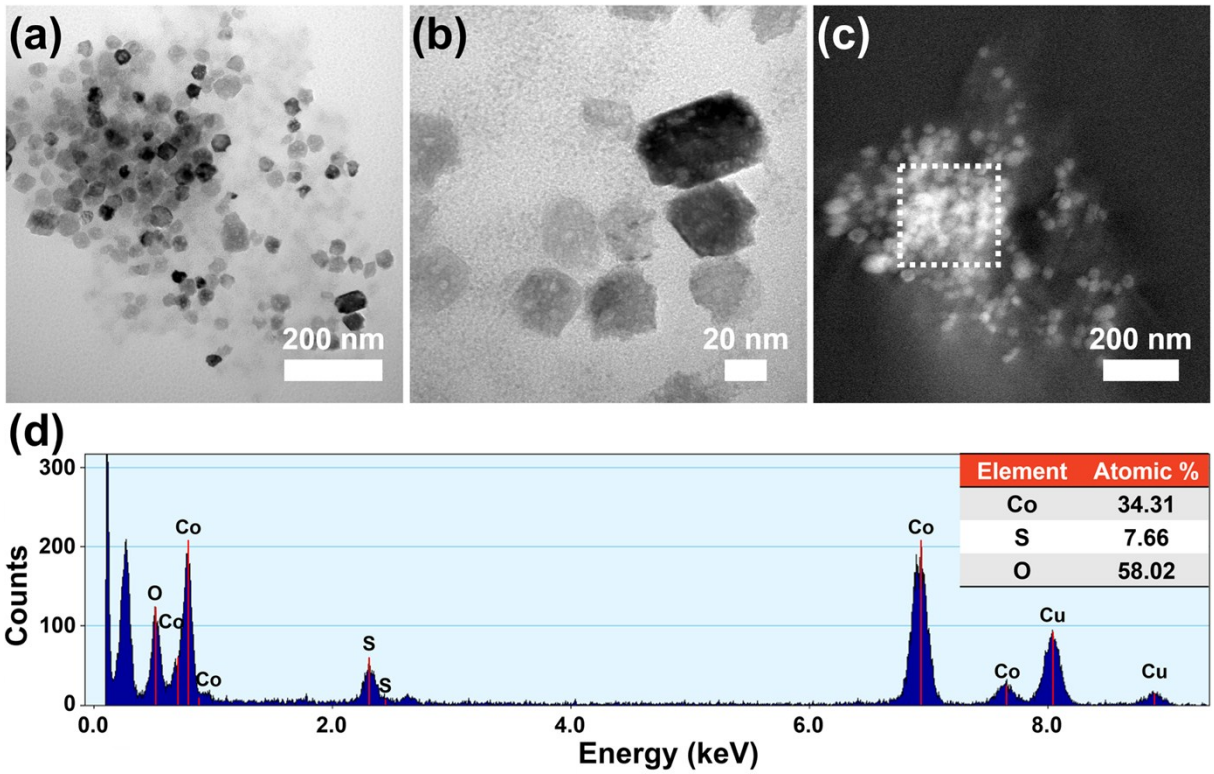

Fig. S4 (a,b) TEM images and (c) STEM image of CoO octahedra after sulfidation in 1-octadecene**.** (d) EDS for the selected area in (c) (Cu detection from TEM grid).

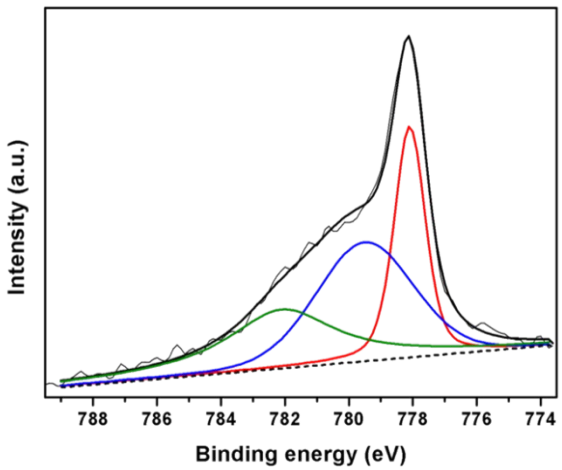

Species	Transition	Binding erengy (eV)	Peak area (%)
Co(0)	$2p_{3/2}$	778.1	28.1
Co(II)	$2p_{3/2}$	780.0	40.6
Co(II)	$2p_{3/2}$	782.1	31.3

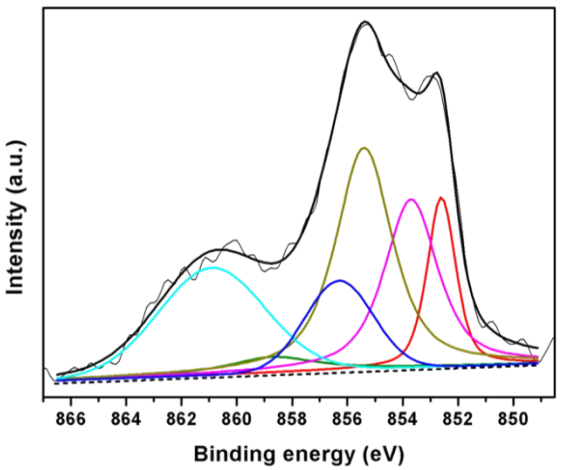

Species	Transition	Binding erengy (eV)	Peak area (%)
Ni(0)	$2p_{3/2}$	852.6	10.9
Ni(0)	$2p_{3/2}$	856.3	11.2
Ni(0)	$2p_{3/2}$	858.7	3.9
Ni(II)	$2p_{3/2}$	853.7	22.0
Ni(II)	$2p_{3/2}$	855.4	30.5
Ni(II)	$2p_{3/2}$	860.9	21.5

Fig. S5 XPS spectra for (a) Co_9S_8 ONC and (b) Ni_9S_8 ONC, and the corresponding tables listing relative peaks areas for deconvoluted XPS peaks.

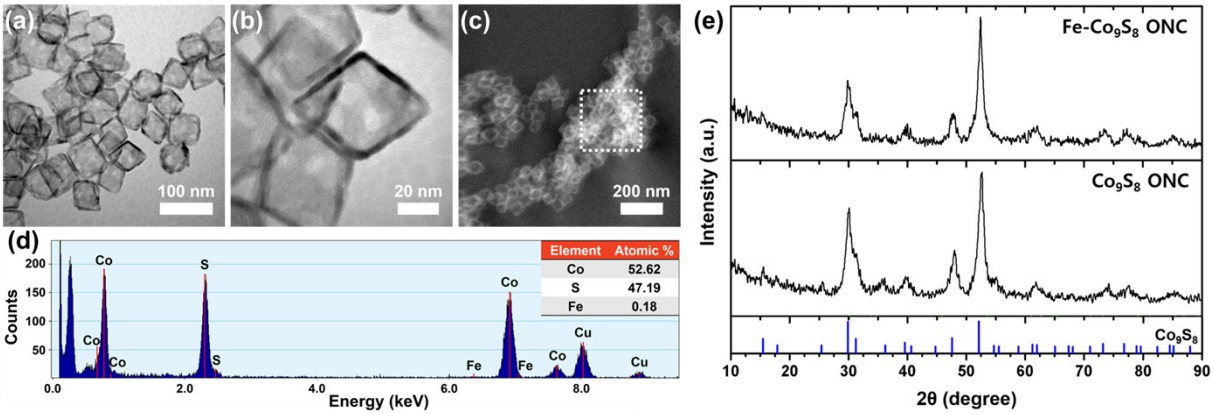

Fig. S6 (a,b) TEM images and (c) STEM image of Fe-Co_9S_8 ONC. (d) EDS spectrum of Fe-Co_9S_8 ONC for the selected area in (c) (Cu detection from TEM grid). (e) XRD patterns of Fe-Co_9S_8 ONC and Co_9S_8 ONC (Co_9S_8, JCPDS #01-086-2273).

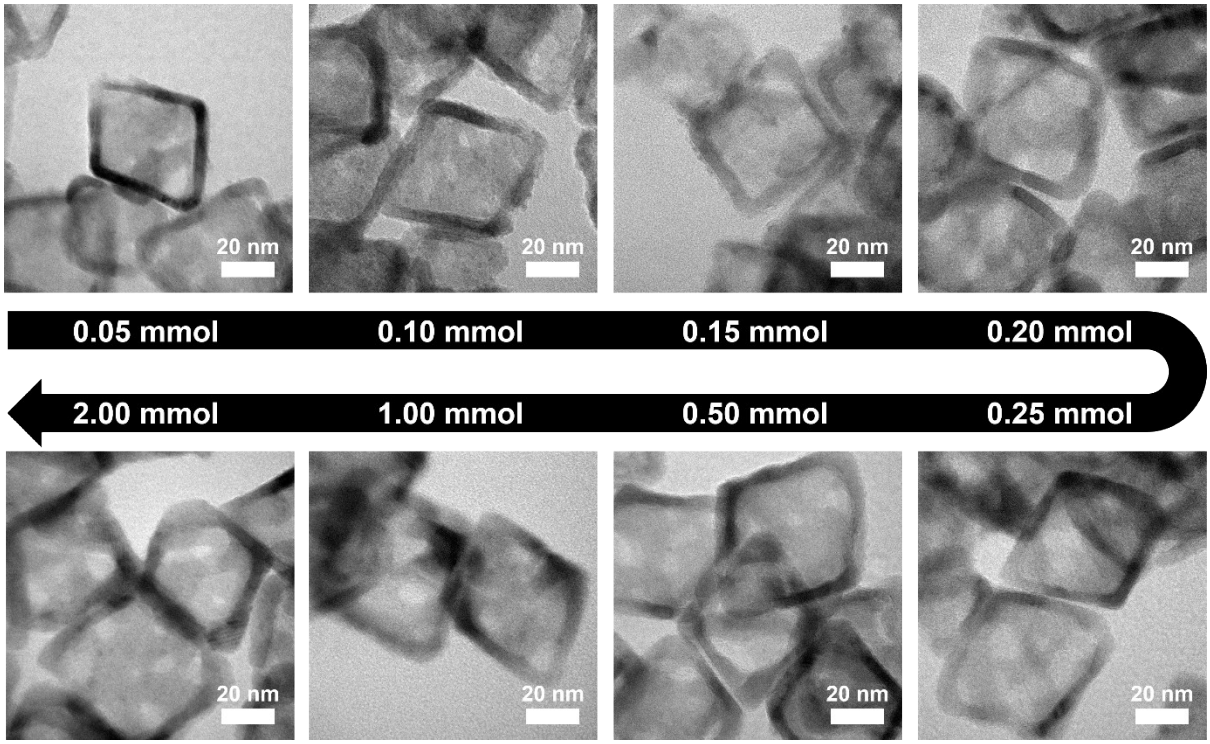

Fig. S7 TEM images showing the phase transformation from Co_9S_8 to Ni_xS_y phases depending on the amount of Ni precursor.

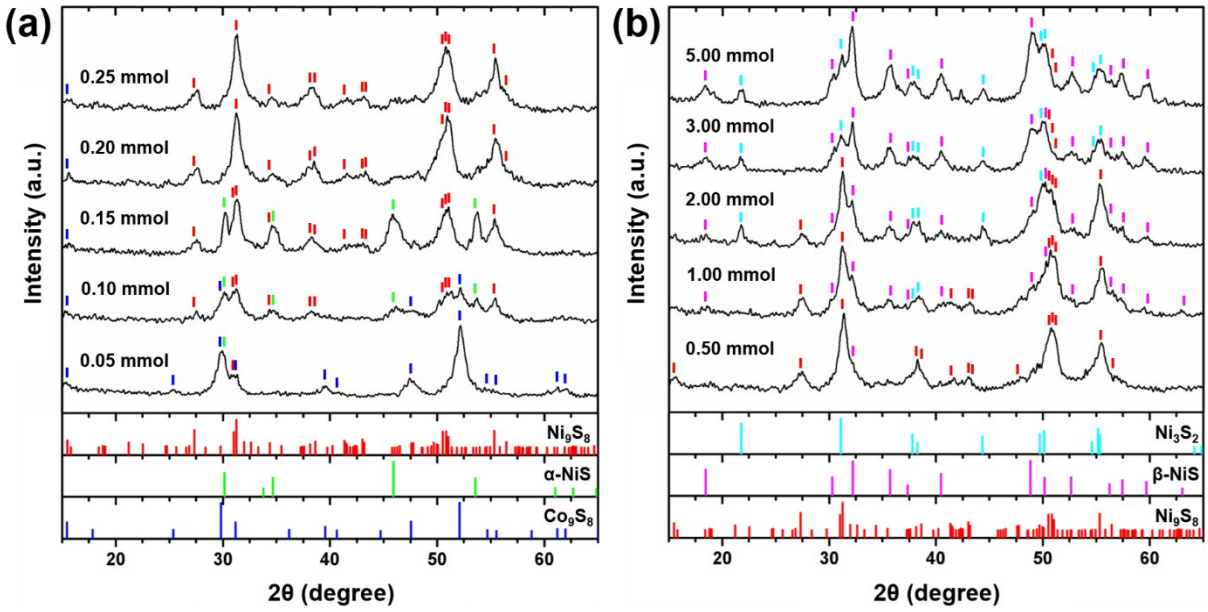

Fig. S8 XRD patterns of the mixed phases of cobalt and nickel sulfides synthesized by adjusting the amount of Ni precursor. (a) From the bottom, the XRD patterns for products by using 0.05 mmol, 0.10 mmol, 0.15 mmol, 0.20 mmol, and 0.25 mmol of Ni precursor. (b) From the bottom, the XRD patterns for products by using 0.50 mmol, 1.00 mmol, 2.00 mmol, 3.00 mmol, and 5.00 mmol of Ni precursor.

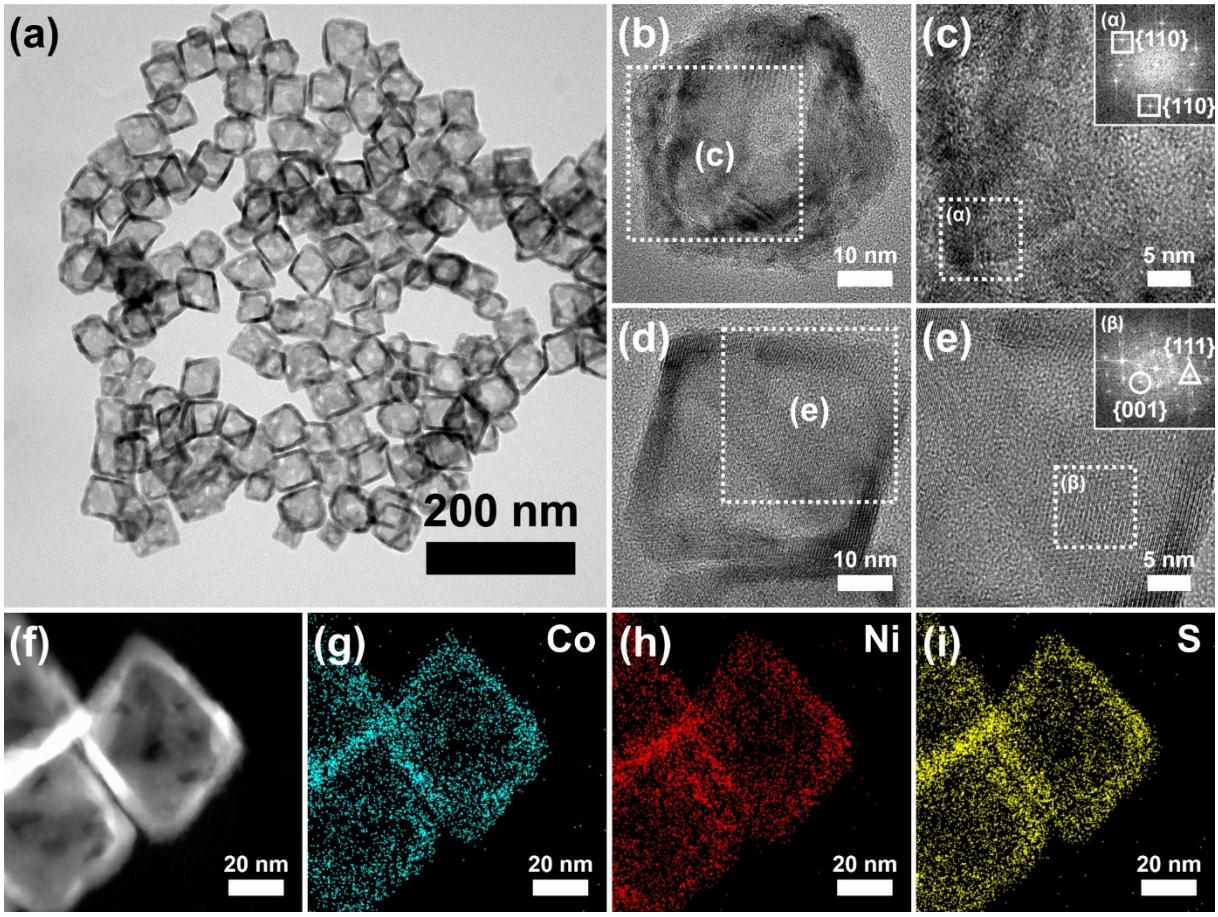

Fig. S9 (a) TEM image and (b-e) HRTEM images of $Co_{9-x}Ni_xS_8$ ONC with (α,β) FFT patterns for the selected areas showing {110}, {111} and {001} facets. (f) STEM image and (g-i) elemental mapping images of $Co_{9-x}Ni_xS_8$ ONC.

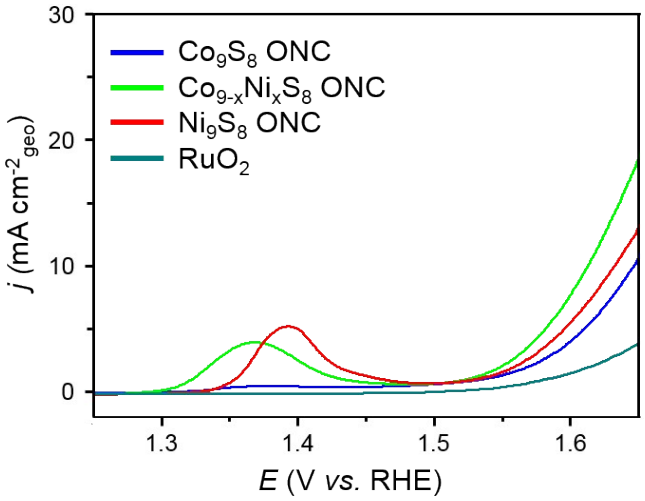

Fig. S10 Linear sweep voltammetry curves presented without *iR*-correction for Co_9S_8 ONC, $Co_{9-x}Ni_xS_8$ ONC, Ni_9S_8 ONC, and 20 wt% RuO_2/C measured in 1 M NaOH at a scan rate of 5 mV s^{-1}.

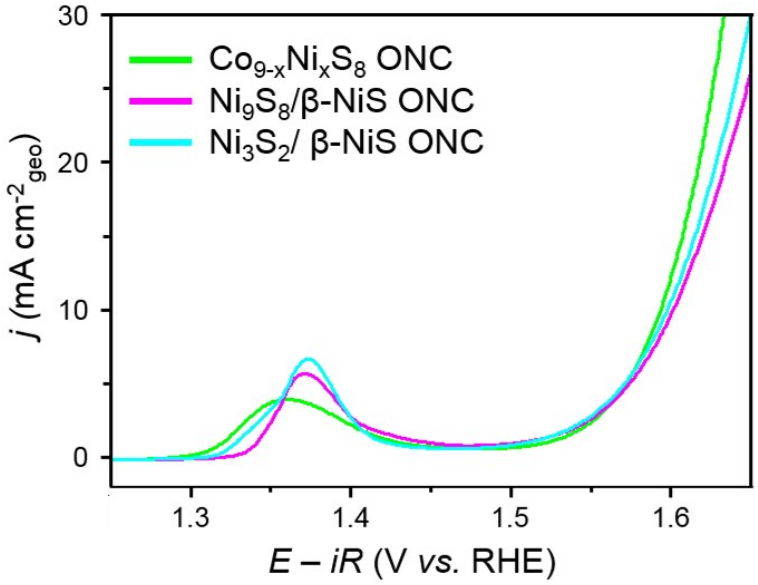

Fig. S11 Linear sweep voltammetry curves of $Co_{9-x}Ni_xS_8$ ONC, Ni_9S_8/β-NiS ONC, and Ni_3S_2/β-NiS ONC, measured in 1 M NaOH at a scan rate of 5 mV s^{-1}. The polarization curves are *iR*-compensated.

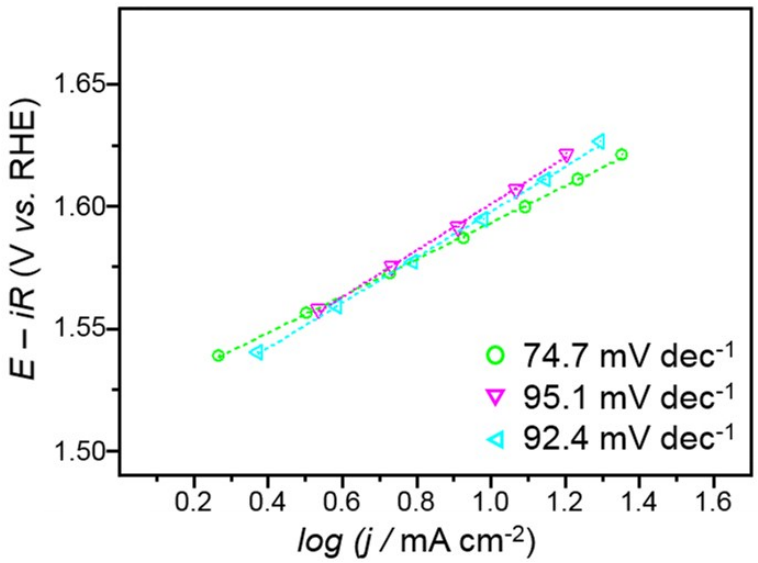

Fig. S12 Tafel plots for $Co_{9-x}Ni_xS_8$ ONC (green circle), Ni_9S_8/β-NiS ONC (magenta triangle), and Ni_3S_2/β-NiS ONC (cyan triangle).

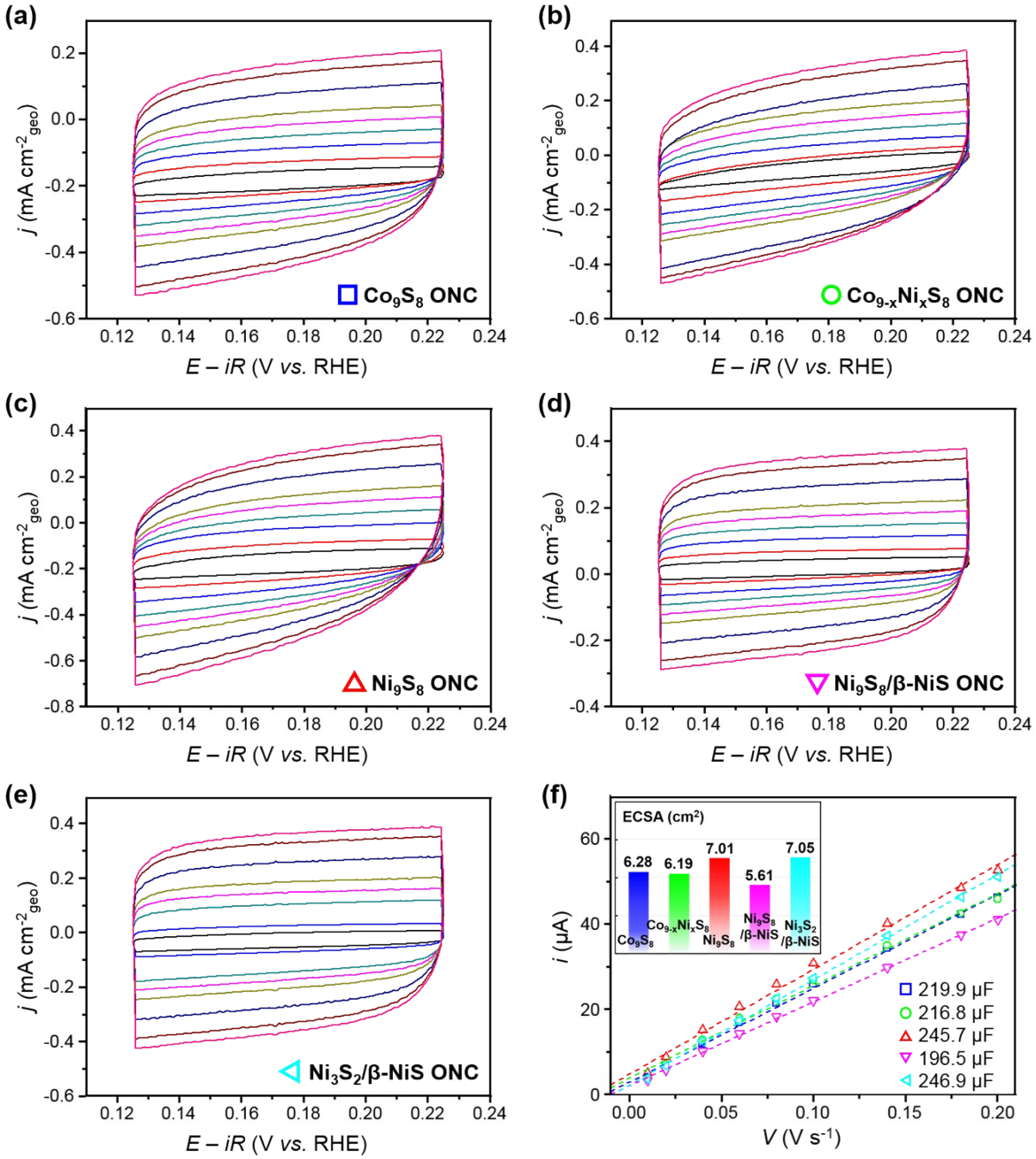

Fig. S13 Electrochemically active surface area by measuring double layer capacitances. Cyclic voltammetry scans with different scan rates (0.01, 0.02, 0.04, 0.06, 0.08, 0.1, 0.14, 0.18, 0.2 V s^{-1}) for (a) Co_9S_8, (b) $Co_{9-x}Ni_xS_8$, (c) Ni_9S_8, (d) Ni_9S_8/β-NiS, and (e) Ni_3S_2/β-NiS ONC. (f) Anodic charging currents measured at 0.175 V vs. RHE as a function of scan rate to measure double layer capacitances and corresponding ECSA values in the inset.

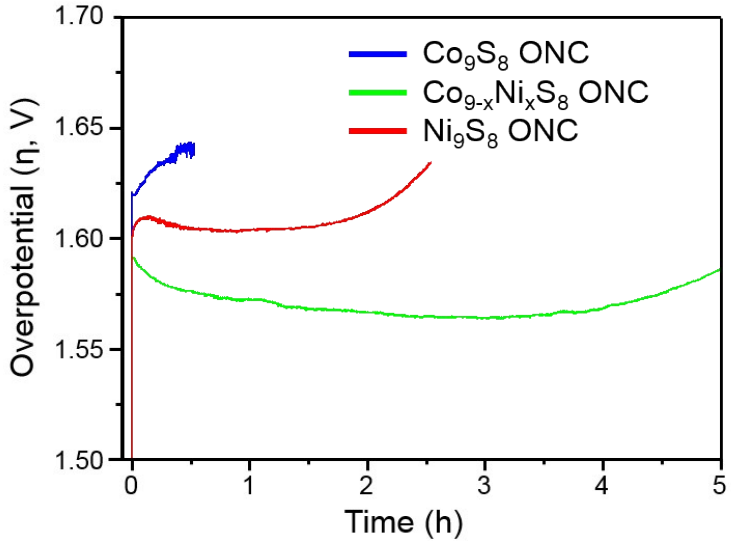

Fig. S14 Chronopotentiometric curves for Co_9S_8 (blue), $Co_{9-x}Ni_xS_8$ (green), and Ni_9S_8 ONC (red) over 5 hours at a contant current density of 10 mA cm^{-2}_{geo}.

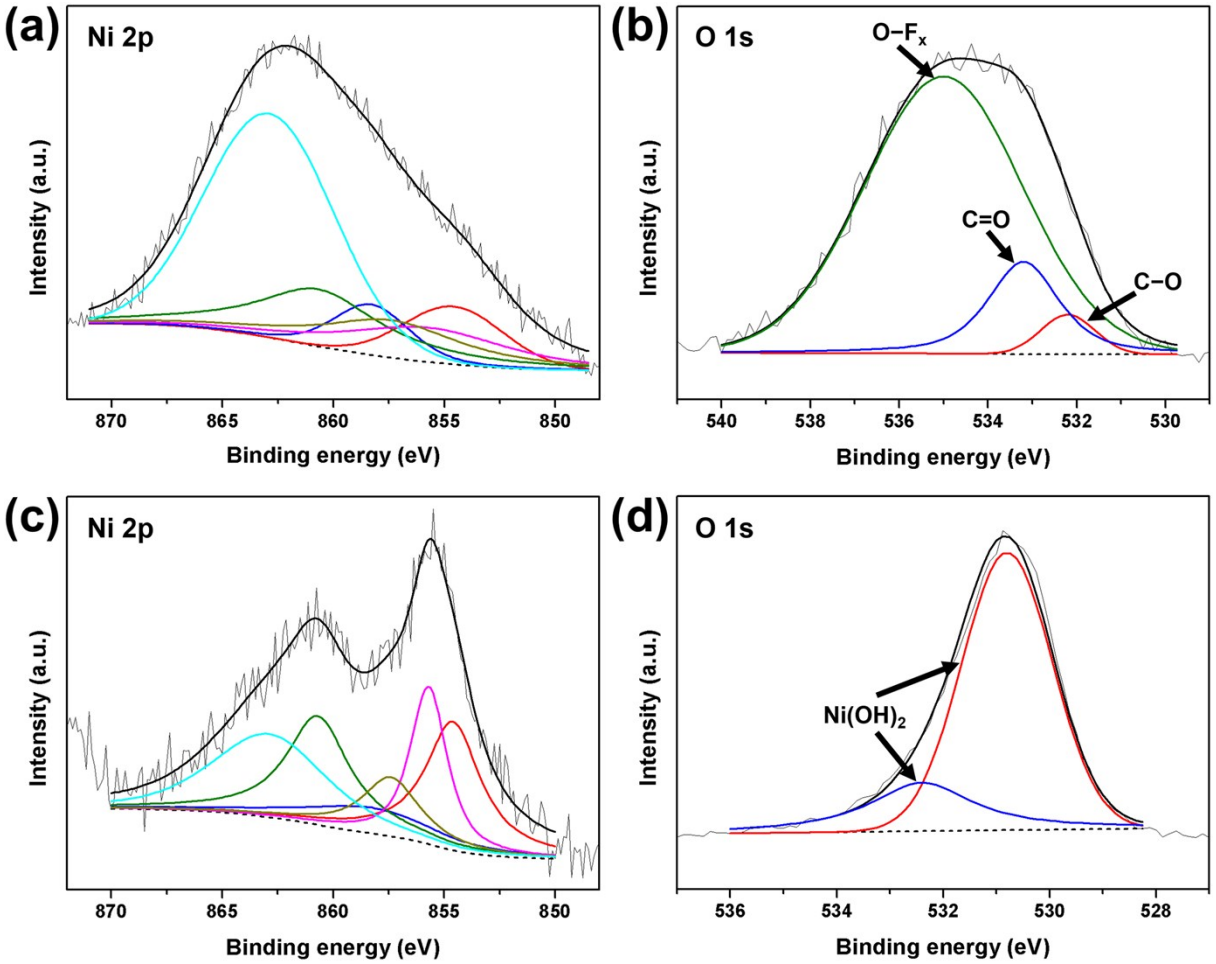

Fig. S15 Deconvoluted XPS spectra for (a) Ni 2p and (b) O 1s of $Co_{9-x}Ni_xS_8$ ONC before electrocatalysis, and (c) Ni 2p and (d) O 1s after 1 h of chronopotentiometry at 10 mA cm^{-2}_{geo}. For (a) and (c), Ni(0) peaks are at 854.6 eV (red), 858.3 eV (blue) and 860.7 eV (green), and Ni(II) at 855.7 eV (magenta), 857.4 eV (dark yellow) and 862.9 eV (cyan).

Supplementary Tables

Phase	Crystal structure	a (α)	b (β)	c (γ)
Co_9S_8	cubic	9.923 (90°)	9.923 (90°)	9.923 (90°)
Ni_9S_8	orthorhombic	9.3359 (90°)	11.2185 (90°)	9.43 (90°)
α-NiS	hexagonal	3.42 (90°)	3.42 (90°)	5.3 (120°)
CoS	hexagonal	3.384 (90°)	3.384 (90°)	5.196 (120°)
β-NiS	rhombohedral	9.619 (90°)	9.619 (90°)	3.1499 (120°)
Ni_3S_2	rhombohedral	5.7465 (90°)	5.7465 (90°)	7.1349 (120°)

Table S1. Crystal structures and lattice parameters of Co_9S_8 (JCPDS #01-086-2273), Ni_9S_8 (JCPDS #01-078-1886), α-NiS (JCPDS #01-075-0613), CoS (JCPDS #01-070-2864), β-NiS (JCPDS #01-086-2281), and Ni_3S_2 (JCPDS #01-085-1802).

Facet	Co_9S_8 (nm)	Ni_9S_8 (nm)	$Co_{9-x}Ni_xS_8$ (nm)
(440)	0.17542	0.17940	0.1777
(002)	0.49615	0.47150	0.4866
(222)	0.28645	0.28577	0.2864

Table S2. Theoretical *d*-spacing values of Co_9S_8 and Ni_9S_8, and the measured *d*-spacing values of $Co_{9-x}Ni_xS_8$ ONC from the FFT patterns of the HRTEM images in Figure S8.